Research Article

Received: 1 December 2022 Revised: 27 March 2023 Accepted article published: 20 May 2023 Published online in Wiley Online Library: 6 June 2023

(wileyonlinelibrary.com) DOI 10.1002/ps.7564

A high adhesion co-assembly based on myclobutanil and tannic acid for sustainable plant disease management

Xuan Li,[a,b] Zhiyuan Zhou,[a,b] Yuqi Huang,[a,b] Gang Tang,[a,b] Yulu Liu,[a,b] Xi Chen,[a,b] Guangyao Yan,[a,b] Huachen Wang,[a,b] Xiaohong Zhang,[a,b] Jialu Wang[a,b] and Yongsong Cao[a,b*]

Abstract

Background: Pesticides are irreplaceable inputs for protecting crops from pests and improving crop yield and quality. Self-assembly nanotechnology is a promising strategy by which to develop novel nano-formulations for pesticides. Nano-formulations improve the effective utilization of pesticides and reduce risks to the environment because of their eco-friendly preparation, high drug loading, and desirable physicochemical properties. Here, to enhance the utilization efficiency of myclobutanil (MYC) and develop a novel nano-formulation, carrier-free co-assembled nanoparticles (MT NPs) based on MYC and tannic acid (TA) were prepared by noncovalent molecular interactions using a green preparation process without any additives.

Results: The results showed that the prepared spherical nanoparticles had good stability in neutral and acidic aqueous solutions, low surface tension (40.53 mN m^{-1}), high rainfastness, and good maximum retention values on plant leaves. Release of active ingredients from MT NPs could be regulated by altering the molar ratio of subassemblies in the co-assembly and the pH of the environment. Antifungal experiments demonstrated that MT NPs had better activities against *Alternaria alternata* and *Fusarium graminearum* [half-maximal effective concentration (EC_{50}) = 6.40 and 77.08 mg/L] compared with free MYC (EC_{50} = 11.46 and 124.82 mg/L), TA (EC_{50} = 251.19 and 503.81 mg/L), and an MYC + TA mixture (EC_{50} = 9.62 and 136.21 mg/L). These results suggested that MYC and TA incorporated in the co-assembled nanoparticles had a synergistic antifungal activity. The results of a genotoxicity assessment indicated that MT NPs could reduce the genotoxicity of MYC to plant cells.

Conclusion: Co-assembled MT NPs with synergistic antifungal activity have outstanding potential for the management of plant diseases.

Keywords: myclobutanil; tannic acid; co-assembly; nanoparticles; plant disease

1 INTRODUCTION

Pesticides are irreplaceable inputs for protecting crops from pests and improving crop yield and quality in modern agriculture.[1,2] However, ultraviolet (UV) degradation, low leaf deposition, and the loss of pesticides through rain wash-off not only lead to a low effective utilization rate of pesticides, but are also potential threats to the ecological environment.[3–6] Nano-based carrier systems for pesticide formulations have been rapidly developed to resolve these problems because of their small size effects and flexible targeted delivery.[7–9] The structure and surface chemistry of nanocarriers can be modified to provide pesticide properties and functions such as good penetration, high surface activity, and intelligent transmission, which enable pesticide delivery to the desired location in plants.[10–12] Although nanocarrier systems can improve the control effect of pesticides to a certain extent, some problems remain to be solved for practical applications, such as the incomplete exposure of active ingredients, non-degradation of the carrier, high material cost, low loading capacity, and complex modification synthesis.[13–16]

Self-assembled nanotechnology, a promising strategy by which to develop novel nano-formulations of drugs, has obvious advantages such as a high load efficiency, no vector-induced toxicity, excellent delivery efficiency, and the selective accumulation of active ingredients at target sites.[17–20] Self-assembled nanoparticles (NPs) can be prepared using simple and green methods through noncovalent molecular interactions, including π–π stacking, hydrogen bonding, host–guest interactions, electrostatic forces, hydrophobic interactions, and van der Waals force, without using environmentally harmful chemicals.[21–23] In our previous work, co-assembled NPs based on the fungicides fenhexamid and polyhexamethylene biguanide were constructed via electrostatic

* Correspondence to: Y Cao, No. 2 Yuanmingyuan West Road, China Agricultural University, Beijing, 100193, China. E-mail: caoysong@126.com; caoys@cau.edu.cn

a College of Plant Protection, China Agricultural University, Beijing, China

b Sanya Institute of China Agricultural University, Sanya, China

and hydrophobic interactions in aqueous solution, and the achieved co-assembly had desirable physicochemical properties and a synergistic effect on the antimicrobial activity.[24] Spinosad and sulfamic acid have been assembled to give stable and orderly NPs in aqueous solution via noncovalent interactions without the use of any chemical additive, and the obtained NPs showed better insecticidal activity than free spinosad.[25] A carrier-free co-assembly based on two natural fungicides, curcumin and berberine, was prepared using a simple and rapid procedure (solvent exchange method), and the prepared submicron particles showed desirable photoactivated antibacterial activity.[26] Prodrugs were prepared by conjugating fipronil and pyrimethanil with inversely polar groups and subsequently self-assembled into a regular nano-structure to obtain prodrug-based self-assemblies by intramolecular polar balancing forces. The prepared assemblies showed improved physicochemical properties, bioactivities, and reduced toxicities toward non-target organisms.[27,28] Therefore, self-assembled drug delivery systems have excellent potential applications because of their eco-friendly preparation, high drug loading, and desirable physicochemical properties.

Myclobutanil (MYC, alpha-butyl-alpha-(4-chlorophenyl)-1*H*-1,-2,4-triazole-1-propanenitrile), one of the triazole fungicides, has been widely applied to control *F. graminearum* and *Alternaria nee* in vegetables, fruits, and crops by inhibiting sterol biosynthesis and damaging cell membrane function.[29,30] Commercial formulations of MYC are emulsifiable concentrates and wettable powders, and practical application of these formulations is limited due to the photo-instability and weak rainfastness of MYC.[31,32] Tannic acid (TA), found in berries, vegetables, olives, cocoa, and other plants with excellent hydrophilic, anti-inflammatory, antioxidant, and antifungal activities, is one of the most abundant polyphenols in nature.[33–35] It has been used in pharmaceutical chemistry as a multifunctional molecule owing to its strong affinity to biological macromolecules and drugs such as insoluble extracellular matrices, peptides, and doxorubicin.[36–38] The chemical mechanism by which TA binds to many drugs involves phenolic hydroxy-rich moieties [five galore groups (three -OH groups bound to an aromatic ring) and five catechol groups (two -OH groups covalently linked to an aromatic ring)] that form multiple hydrogen bonds to produce hydrophobic interactions with target molecules.[39–41]

Here, to develop a novel nano-formulation to improve the utilization efficiency of MYC, high adhesion co-assembled nanoparticles (MT NPs) based on MYC and TA were prepared by a noncovalent molecular recognition method using a green preparation process. The effects of molar ratio, temperature, pH, and salt concentration on the assembly rate of MT NPs were investigated to optimize the preparation conditions. The prepared MT NPs were characterized by mean particle size, scanning electron microscopy (SEM), transmission electron microscopy (TEM), ultraviolet spectrophotometry, nuclear magnetic resonance (NMR), Fourier transform infrared (FTIR), thermogravimetry and differential scanning calorimetry (TG–DSC). Furthermore, the light stability, surface tensions, maximum retention on different plant leaves, rainfastness (resistance to rain erosion), controlled release behavior, antifungal activity, and genotoxicity of the MT NPs were fully estimated.

2 MATERIALS AND METHODS

2.1 Materials

Myclobutanil technical (MYC, 98.5%) and myclobutanil wettable powder (MYC WP, 400 g/kg) were supplied by Shandong United Pesticide Industry Co., Ltd (Taian, China). Magnesium sulfate (99%), sodium chloride (99%), hydrochloric acid (37%), calcium chloride (99%), sodium hydroxide (NaOH, 99%), potassium dihydrogen phosphate (99.5%), dipotassium hydrogen phosphate (99%), TA, and dimethylsulfoxide (DMSO) were purchased from Aladdin Industrial Corporation (Shanghai, China). Dialysis bags [molecular weight cut-off (MWCO) 2000 Da] were from Shanghai Macklin Biochemical Co., Ltd. (Shanghai, China). The acetonitrile was high-performance liquid chromatography (HPLC) grade (J.T. Baker, USA). Deionized water (18 MΩ cm^{-1}) was prepared using a water purification system (Millipore, Milford, MA, USA) for all reactions and treatments. Separation and analysis were performed on a reversed-phase Kromasil ODS C_{18} column (250 mm × 4.6 mm, 5 μm) using a Shimadzu HPLC system and the column temperature was 25 °C. The mobile phase consisted of water (eluent A) and acetonitrile (eluent B) (20:80, v/v) at a flow rate of 1 mL/min. The injection volume was 20 μL, and the detection wavelengths of MYC and TA were 214 nm and 276 nm, respectively. Fungi (*Alternaria alternate and F. graminearum*) were provided by the Laboratory of Seed Pathology and Fungicide Pharmacology at China Agricultural University (CAU, Beijing, China).

2.2 Methods

2.2.1 Preparation

The solvent exchange method was used to prepare co-assembled NPs. A mixture of MYC and TA was dissolved in DMSO at the desired molar ratio, dispersed well in water and stirred at 600 rpm for 30 min. The resulting solution was dialyzed in a poly(vinylidene fluoride) dialysis bag (MWCO: 2000 Da) for 24 h to remove unassembled MYC, TA, and organic solvents, and the retained solution in the dialysis tube was then lyophilized to obtain MT NPs. The co-assembly rate (*CAR*) of MT NPs was calculated as:

$$CAR\,(\%) = N_t/N_0 \times 100\% \quad (1)$$

Where N_0 is the initial amount of MYC and N_t is MYC reserved in the dialysis tube.

2.2.2 Morphology

A scanning electron microscope (S4800, Hitachi, Japan) and transmission electron microscope (JEM-1230, JEOL, Tokyo, Japan) were used to observe the morphology of MT NPs. The particle size and polydispersity index (PDI) distribution of MT NPs in aqueous solution were measured by laser particle-size analysis (Mastersizer 3000, Malvern Instruments, UK).

2.2.3 Spectral characterization and thermal behavior

The UV-visible absorption spectra of the samples were obtained using a UV-visible spectrophotometer (Genesys180, Thermo Fisher Scientific, USA). ^{1}H NMR spectra were recorded using a Bruker AVANCE III HD 400 MHz NMR spectrometer (Bruker, Germany) with tetramethylsilane as the internal standard and deuterium oxide (D_2O) and chloroform-*d* ($CDCl_3$) as solvents. FTIR data were recorded using a Tensor 27 spectrophotometer (Bruker) to identify different functional groups in the MT NPs. The TG–DSC method (STA 449F3, NETZSCH, Germany) was used to study the thermal stability of the MT NPs.

2.2.4 Photostability

The photostability of MT NPs was evaluated with reference to our previous work.[26] To assess the photostability of MT NPs under UV

light, quartz tubes filled with a suspension of MT NPs (containing 9 mg/L of MYC) were placed under a 300 W (E_{max} = 365 nm) UV lamp at a distance of 20 cm under environmental conditions. At various time intervals, 500-μL samples were taken from each tube, and the concentration of MYC was analyzed by HPLC.

2.2.5 *Surface activity*

The surface activities of different samples (MYC, TA, and MT NPs) were measured using a JK 99B analyzer (Powereach, China; resolution <0.05 mN m^{-1}) at 25 °C. The sensing platinum plate was heated to dryness after rinsing in distilled water and was slowly placed perpendicular to the liquid sample interface. As the liquid interfacial tension and other related forces were brought to equilibrium, interfacial tension was measured. Each treatment was replicated three times.

2.2.6 *Maximum retention of MT NPs on different plant leaves*

The maximum retention of MT NPs was evaluated in the greenhouse on the leaves of eight different plants: *Glycine max*, *Zea mays*, *Lactuca sativa*, *Brassica napus*, *Triticum aestivum*, *Brassica pekinensis*, *Nicotiana benthamian*, and *Lycopersicon esculentum*. Suspensions or aqueous solutions of MYC, TA, and MT NPs were placed separately in beakers at concentrations of 40, 60, and 100 mg/L, respectively. Uniform-sized leaves (area *S*) were separately weighed (W_0) using a precision electronic balance and then immersed in beakers containing aqueous solutions/suspensions of diverse samples under ambient environmental conditions. After 15 s, leaves were quickly removed from the beakers and suspended in air for 3 min. Leaf weight was measured again (W_1). The formula for calculating the maximum retention per unit area was as follows:

$$R_M = (W_1 - W_0)/2 \times S \quad (2)$$

2.2.7 *Controlled release behavior*

The release behaviors of MT NPs with different molar ratios of MYC to TA were investigated using a dialysis method. Typically, a dialysis bag (MWCO: 2000 Da) containing ~ 2 mL of MT NPs suspension was immersed in a conical flask containing 100 mL of phosphate buffer solution (PBS) at different pH (5.0, 7.0, and 9.0). The conical flask was placed on a rotary shaker (100 rpm) in the dark at room temperature (25 ± 1 °C). At a predetermined time, 1.0 mL of the dialysate was sampled for HPLC analysis. The same volume of fresh PBS was replenished each time. The release performance of MT NPs was fitted using the Ritger–Peppas equation:

$$Mt/Mz = kt^n \quad (3)$$

Where *Mt*/*Mz* is the percentage of MYC released from MT NPs at time *t*, *k* is the rate constant, and *n* is the diffusion parameter.

2.2.8 *Rainfastness*

Quantitative measurement of rainfastness on the surface of *T. aestivum* leaf was performed using a simulated rain-washing method.[42] A set of simulated rainwater spraying devices were made by fixing *T. aestivum* leaves ~ 10 cm below the nozzle at an angle of 30° from the horizontal plane, and a Petri dish was placed below the leaves to receive the rainwater after rinsing. First, ~ 500 μL of MYC WP or MT NPs (100 mg/L) suspension was sprayed evenly onto *T. aestivum* leaf surfaces that were subsequently air-dried for ~ 2 h. Then, to simulate rainwater, deionized water was uniformly sprayed on the leaves, resulting in a constant rainfall intensity of 20 mm for 24 h, which is equivalent to moderate rain. Leaves were removed for air-drying after being rinsed for different lengths of time. After being air-dried, leaves were immersed in 10 mL of acetonitrile, shaken at 120 rpm for 10 min, and the remaining MYC on the leaf surface was extracted in acetonitrile solution. Finally, the concentration of MYC in the acetonitrile solution was determined by HPLC. Each treatment was replicated three times.

2.2.9 In vitro *fungicidal activity*

The *in vitro* fungicidal activities of different samples against *Alternaria alternia alternate* and *F. graminearum* were evaluated by using the growth rate of mycelium on potato glucose agar (PDA) plates. The effective concentration (EC_{50}) that inhibits mycelial growth by 50% was calculated for each sample. After regeneration, mycelial discs of phytopathic fungi ~ 5 mm in diameter were inoculated in the center of PDA medium containing samples with different concentrations. Meanwhile, deionized water was added to PDA medium as a blank control. Each treatment was performed in triplicate. When the mycelium completely covered the control dish, the diameter of the colony for each treatment was recorded in two vertical directions.

2.2.10 In vivo *control efficacy*

Early flowering wheat (*T. aestivum* L) plants were used to evaluate the control efficacy of MT NPs against *F. graminearum* in the greenhouse. Wheat seedlings were cultivated in plastic pots containing nutrition soil in the greenhouse. The temperature was 15–23 °C, and the photoperiod was 13:11 h light/dark. Suspensions of different sample concentrations were applied to the wheat seedlings under ambient temperature during the early flowering period. A conidia inoculum of *F. graminearum* with 0.01% of Tween 20 added was then sprayed evenly on the seedling ears. Wheat seedlings were cultivated in a growth cabinet with a 16:8 h light/dark photoperiod, a day/night temperature of 25/17 °C, and relative humidity of 85%. Diseased ear rates were determined for *F. graminearum* at 21 days and each treatment had three replications.

2.2.11 *Genotoxicity evaluation*

Vicia faba bio-assay is an efficient plant bio-assay that is extensively used in the genotoxicity assessment of pesticides and other chemical substances.[43] The genotoxicities of MYC, TA, and co-assembled MT NPs to root tip cells of *V. faba* were investigated. First, broad bean seeds were soaked in water for 24 h, removed from the water and wrapped in a wet towel at normal temperature until the new roots had grown to 1–2 cm. Root tips immersed in different concentrations of sample suspensions for 24 h were then transferred to deionized water and cultivated for another 24 h. After treatment, roots were gathered and fixed with an acetic acid/ethanol mixture (1:3, v/v) at 23 °C for 24 h. After being rinsed three times with deionized water, the cells were cultivated in HCl (1 M) solution at 60 °C for 8 min. Finally, 2 mm of the apical meristematic region for each treatment was placed on a slide and stained with 100 μL of carbol fuchsin. The colored roots were squashed and covered with coverslips for cytological analysis. Approximately 1000 cells per slice were observed under an optical microscope (Olympus Japan Co. Ltd., Japan). Deionized water was used as a blank control. Each treatment was replicated three

times. The micronucleus frequency and mitotic index (proportion of cells in division) of the *V. faba* root tip cells were calculated.

2.2.12 *Statistical analysis*

Statistical analysis was carried out using SPSS 23.0 statistical analysis software. The data were fitted and analyzed using Microsoft Office Excel 2021 and Origin 2022. All experimental data were presented as mean ± standard deviation.

3 RESULTS AND DISCUSSION

3.1 The co-assembly formation

Scheme 1 indicates the possible formation mechanism of co-assembled MT NPs. First, water-insoluble MYC and water-soluble TA were dissolved in DMSO and converted to the molecular state under high-speed stirring. When the mixed solution was added to the aqueous solution, the polar solvent DMSO interacted with the water molecules resulting in the slow precipitation of MYC from the aqueous solution. During the sedimentation of MYC, TA could attract and interact with the MYC molecules through noncovalent interactions such as hydrogen bonds, π–π stacking, and hydrophobic forces because of the special unguiculate molecular structure of TA. The molecules might then rotate and intertwine through noncovalent interactions to form spherical three-dimensional structures in which hydrophobic MYC might form the core and hydrophilic TA might form the shell, leading to an orderly arrangement of core–shell structures dispersed in water. When MYC and TA were co-assembled entirely in water, the resulting solution showed an obvious Tyndall phenomenon with a particle size of 143 nm.

3.2 Preparation

3.2.1 *Effect of pH on the* CARs *of MT NPs*

pH might be the main factor that affects intermolecular forces such as hydrogen bonds, π–π stacking, and hydrophobic force. Figure 1(A) shows the *CAR* and size distribution characteristics of MT NPs at different pH values of 2, 5, 7, 9, and 11. When the pH was 2, 7, 9, and 11, the *CAR* values were < 60% and most MYC could not form NPs and precipitated out. At pH 5, a translucent colloidal solution forms and an evident Tyndall phenomenon can be observed; an assembly rate of 81.55% was achieved. The results showed that the co-assembly of TA and MYC was pH-dependent. Possible reasons for this result are that TA was in the molecular and anion forms in neutral and alkaline aqueous solutions (pH 7, 9, and 11) respectively, and interactions between TA and MYC were weak, resulting in lower *CAR* values. TA existed completely in the proton form in the strong acid solution (pH 2), and the low *CAR* value might be because the strong exclusion force among protons was greater than the attraction between TA and MYC. In the pH 5 solution, TA was in the molecular and proton forms simultaneously, which could attract and interact with the MYC molecule through noncovalent interactions such as hydrogen bonds, π–π stacking, and hydrophobic forces resulting in a higher *CAR* value. Therefore, pH 5 is optimal for the co-assembly of MYC and TA in aqueous solution.

3.2.2 *Effect of molar ratio on the* CARs *of MT NPs*

The molar ratio of MYC to TA also had a great effect on co-assembled MT NPs driven by noncovalent interactions. As shown in Fig. 1(B), when the molar ratio of MYC to TA was 7:1, 8:1, 10:1, and 11:1 at pH 5 in aqueous solution, the *CAR* of MT NPs was 64.8%, 72.2%, 64.6%, and 52.1% respectively. When the molar ratio of MYC to TA was 9:1, the *CAR* of MT NPs was 82.40% and the average size of MT NPs was smaller than that at other molar ratios of MYC to TA, in which a very low PDI value (0.013) was achieved, suggesting an extremely stable nanosystem. The reason for this might be that the positive charge of the triazole group in MYC was almost equal to the negative charge of the phenolic hydroxyl groups in TA resulting in the strongest interaction between MYC and TA when the molar ratio of MYC to TA was 9:1. Therefore, the optimal molar ratio of MYC to TA was selected as 9:1 in an aqueous solution at pH 5.

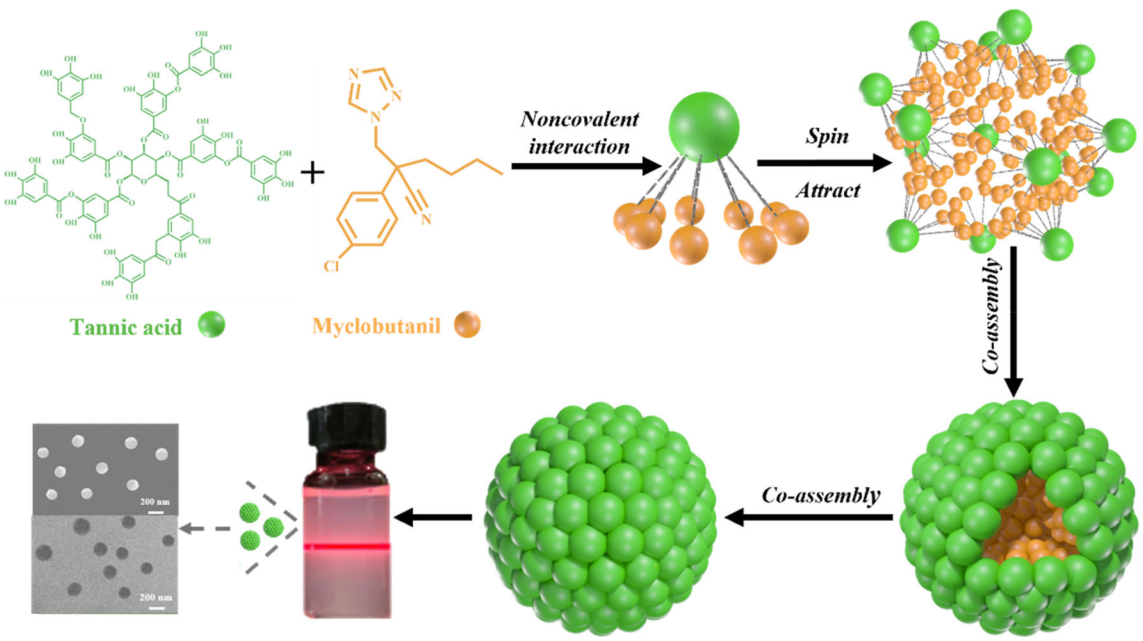

Scheme 1. Possible formation mechanism of carrier-free co-assembled nanoparticles.

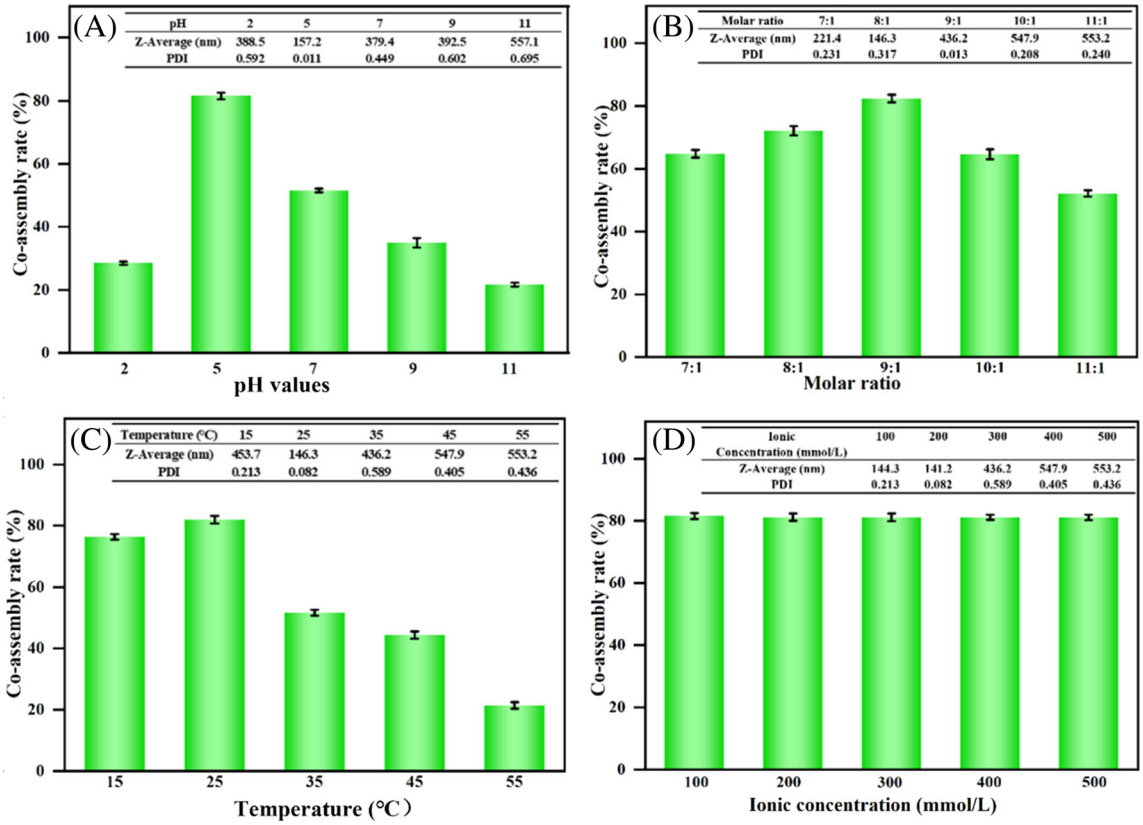

Figure 1. The influences of pH value, molar ratio, temperature, and ionic concentration on the formation of carrier-free co-assembled nanoparticles (MT NPs): pH values of 2, 5, 7, 9, and 11 in deionized water (A); molar ratios of 7:1, 8:1, 9:1, 10:1, and 11:1 in deionized water at pH 5 (B); temperature of 15, 25, 35, 45 and 55 °C in deionized water at pH 5 with a molar ratio of 9:1 (C); molar ratio of 9:1 in 100, 200, 300, 400, and 500 mmol L^{-1} of phosphate-buffered saline at pH 5 and 25 °C (D).

3.2.3 *Effect of temperature on the* CARs *of MT NPs*

The temperature of the aqueous solution also had an important influence on the co-assembled MT NPs. As shown in Fig. 1(C), keeping the molar ratio of MYC to TA at 9:1, pH 5, the *CAR* values of MT NPs were 81.92%, 51.62%, 44.31%, and 21.36% at 25, 35, 45, and 55 °C respectively. This illustrated that the *CAR* values of MT NPs were negatively correlated with temperature. This might be because with an increase in temperature, the molecular motion of TA and MYC in the solution accelerated, leading to partial disintegration of the co-assembled MT NPs. There was no significant difference in the *CAR* values of MT NPs at 15 and 25 °C, where the formed nanosystem had the smallest average size and the lowest PDI value (0.082). Therefore, the optimal temperature for co-assembly of MYC and TA in aqueous solution was 25 °C.

3.2.4 *Effect of ionic strength on the* CAR *of MT NPs*

Keeping the pH at 5, the molar ratio of MYC to TA at 9:1, and the temperature at 25 °C, the *CAR* values of MT NPs were measured in aqueous solutions at different ionic concentrations to investigate the influence of ionic strength on co-assembly. As shown in Fig. 1(D), there was no significant difference in the *CAR*, average size, and PDI value of MT NPs in pH 5 aqueous solutions of different ionic strengths. Therefore, the inorganic ionic strength has little influence on the co-assembly of MYC and TA. Based on the experimental results, the optimal conditions for the preparation of MT NPs were confirmed. A 2.64 mg quantity of MYC (9.0 μmol) and 1.73 mg of TA (1.0 μmol) were dissolved in 0.5 mL of DMSO in a single-neck round-bottom flask with magnetic stirring for 30 min in the dark. The resulting solution was then slowly added dropwise to 19 mL of pH 5 aqueous solution and magnetically stirred at 25 °C. After being stirred for 30 min, the above solution was transferred to dialysis bags to dialyze for 24 h to remove unassembled MYC, TA, and organic solvent. The solution retained in the dialysis bag was freeze-dried for 72 h to obtain the ideal MT NPs.

3.3 Characterization

The UV-visible absorption spectra of MYC, TA, and MT NPs were measured at 200–400 nm (Fig. 2(A)). TA showed strong absorption peaks at 214 and 276 nm. MYC showed strong absorption peaks at 214 nm. The characteristic absorption peaks (214 nm and 276 nm) of MT NPs contained features of both TA and MYC, demonstrating that MT NPs consisted of MYC and TA. As shown in Fig. 2(B), the FTIR spectra of TA revealed a wider band in the region 3700–3000 cm^{-1} due to –OH stretching vibration in aromatic rings. The bands at 1720, 1610, and 1530 cm^{-1} suggested the presence of a carboxyl group, —C═C— in the aromatic ring. The bands at 1450 cm^{-1} were the deformation of —C—C— in the phenolic group, whereas the band at 1350 cm^{-1} in the TA spectrum was attributed to the phenol group. The band spectrum at 1180 cm^{-1} was due to C–H; additionally, vibration bands at 1130–900 cm^{-1} were attributed to the deformation of C—O and C—H. The bands between 900 and 550 cm^{-1} were due to C—H bonds in the benzene ring. In the FTIR spectra of MYC, the wider band in the region of 3700–3300 cm^{-1} was attributed to C—H.

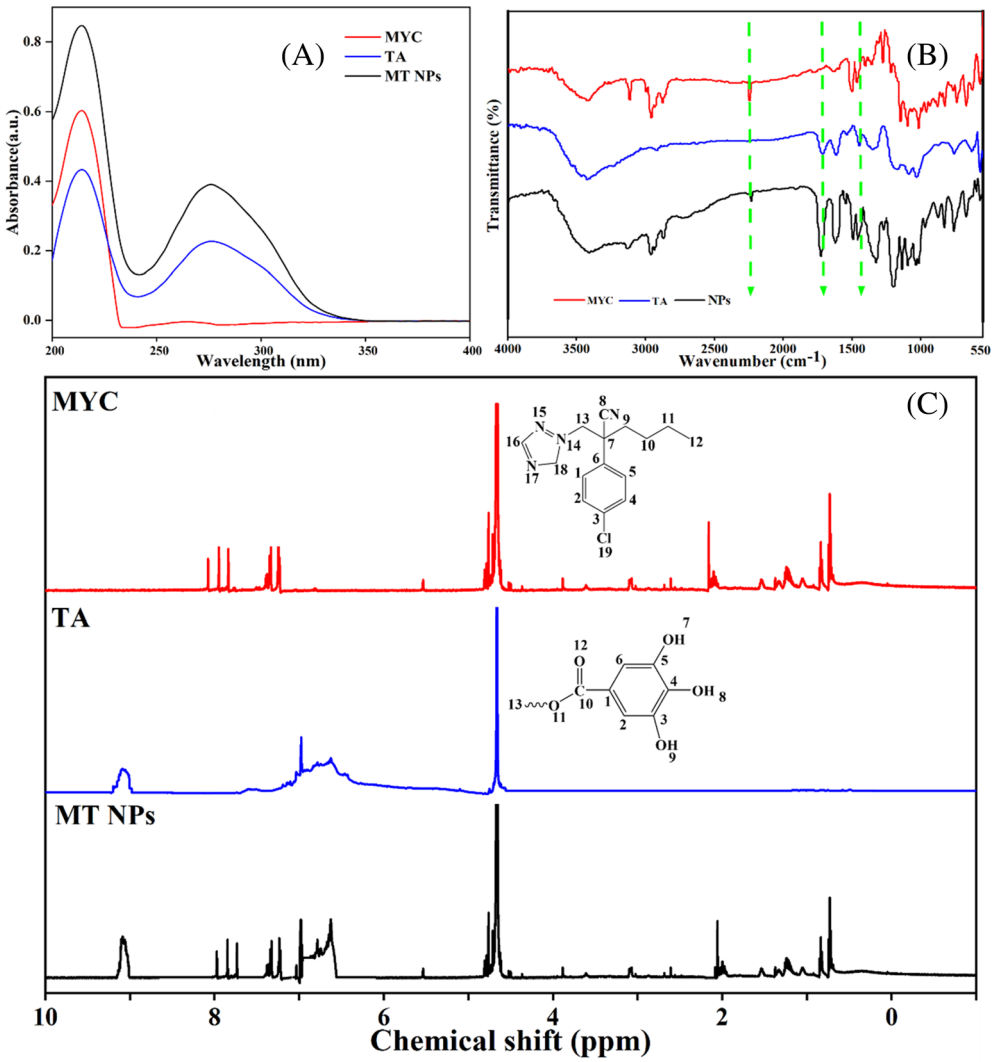

Figure 2. UV-visible absorbance spectra (A), Fourier transform infrared spectroscopy (FTIR) spectra (B) and ^{1}H NMR spectra (C) of myclobutanil (MYC), tannic acid (TA), and carrier-free co-assembled nanoparticles (MT NPs).

The characteristic absorption peaks of MYC at 3110, 2240, 1500, and 1450 cm^{-1} were assigned to the deformation of ═C—H in the aromatic ring, stretching vibration of —C≡N, —C═N— of the triazole ring, and —C═C— of the aromatic ring, respectively. The bands between 1290 and 1250 cm^{-1} were attributed to ═C—N— in the triazole ring. The characteristic absorption bands at 800–550 cm^{-1} were due to the stretching vibration of C—Cl. The characteristic absorption bands of obtained MT NPs were mainly consistent with MYC and TA. Because of the strong hydrogen bonding force between MYC and TA, the band of —C≡N on MYC was shifted to a lower wavenumber in MT NPs from 2240 to 2230 cm^{-1}, and the band of the carboxyl group on TA was shifted to a higher wavenumber in MT NPs from 1720 to 1730 cm^{-1}. Because of the presence of a π–π stacking force between MYC and TA, the band of the —C═N— on MYC was shifted to a lower wavenumber in MT NPs from 1500 to 1490 cm^{-1}, and the band of the —C═C— on TA was shifted to a higher wavenumber in MT NPs from 1450 to 1462 cm^{-1}. Figure 2(C) shows the ^{1}H NMR spectra of MYC, TA, and MT NPs. The results indicated that the chemical shifts of ^{1}H in MYC were located at 7.95, 7.84, 7.52, 7.43, 4.76, 2.10, 1.24, and 0.73 ppm, respectively, and the corresponding integral area ratio was 1:1:2:2:2:2:4:3. The chemical shifts of ^{1}H in TA were located at 8.99 and 6.63 ppm, respectively, and the corresponding integral area ratio was 25:27. Although the chemical shifts of ^{1}H in MT NPs were basically similar to that of MYC and TA, the chemical shift of H-16 of MYC in MT NPs shifted to a low field, from 7.95 to 7.84 ppm; the chemical shift of H-18 of MYC in MT NPs shifted to a low field, from 7.85 to 7.72 ppm; the chemical shifts of H-2 and H-4 of MYC in MT NPs shifted to a low field, from 7.52 to 7.32 ppm; and the chemical shifts of H-1 and H-5 of MYC in MT NPs shifted to a low field, from 7.43 to 7.24 ppm. The chemical shifts of 7-OH, 8-OH, and 9-OH of TA in MT NPs shifted to a high field, from 8.99 to 9.11 ppm and the chemical shifts of H-2 and H-6 of TA in MT NPs shifted to a high field, from 6.63 to 6.79 ppm. According to these obtained results, it can be concluded that the MT NPs were co-assembled by MYC and TA through noncovalent interactions.

3.4 Thermal behavior

Figure 3(A),(C) show the TG, DTG, and DSC curves of MYC, TA, and MT NPs, respectively. In Fig. 3(A), the TG and DTG curves indicate

that the weight loss (~ 99%) of MYC occurred in the temperature range 160–350 °C and the DSC curve shows that the melting point of MYC was ~ 74°C. Figure 3(C) shows that the melting point of TA was 200 °C, the rapid weight loss (~ 49%) of TA with increasing the temperature above 230 °C could be attributed to the decomposition of TA. In Fig. 3(C), the curves show that the rapid weight loss (~ 80%) of MT NPs occurred in the temperature range 170–325 °C and the slow weight loss (~ 13%) of MT NPs occurred in the temperature range 325–600 °C. These phenomena might be due to the interaction between MYC and TA, which improved the decomposition temperature ranges of MT NPs. Therefore, the MT NPs co-assembled by TA and MYC could increase the thermal stability of MYC.

3.5 Morphology

Figure 4(A) indicates that free MYC or free TA could not self-assemble into NPs, and water-insoluble MYC precipitated out in aqueous solution and aggregated as sediment. MYC could co-assemble with TA to form a stable nanosystem with evident Tyndall phenomenon in aqueous solution at pH 5 and 25 °C. The obtained MT NPs had a uniform shape with an average size of 143 nm, and low PDI of 0.092, indicating that the obtained co-assembly had good stability (Fig. 4(B)). SEM and TEM images show that the resulting MT NPs were regular spherical NPs (Fig. 4(C),(D)).

3.6 Photostability

In general, the photo-instability of some pesticides, including MYC, is the main reason for the low utilization of conventional pesticide formulations in practical applications. Figure 5(A) indicates the influence of UV radiation on MYC and MT NPs at 25 °C. The results showed that MYC was very sensitive to light and its photodegradation rate reached ~ 60% after 24 h of UV irradiation. However, the decomposition rate of MYC in MT NPs was only 24.7% under the same conditions. This result indicated that the photostability of MYC in MT NPs was enhanced because of the shielding or adsorption of UV light by TA. Thus, MT NPs with excellent photostability could improve the utilization efficiency of MYC and reduce the dosage of MYC used in practical applications.

3.7 Surface activity and maximum retention

3.7.1 Surface activity

Normally, surfactants are essential to improve the surface activity of conventional pesticide formulations. The surface activity of MT NPs was estimated by measuring the surface tension and maximum retention on the leaves of diverse plants. The surface tensions (mN m^{-1}) of diverse samples are demonstrated in Fig. 5(B). The surface tension of water was highest (71.73), followed by TA (71.45), MYC (49.46), and MT NPs (40.53). TA has little influence on the surface tension of water. Although the presence of MYC could reduce the surface tension of water to some extent, the surface tension of MT NPs was the lowest among all samples. The surface tension of MT NPs decreased with the increasing concentration of MT NPs (Fig. 5(C)). Therefore, the co-assembly of MYC and TA had excellent surface activity without adding any additive.

3.7.2 Maximum retention

The maximum retention of TA, MYC, and MT NPs on surface of *G. max*, *Z. mays*, *Lactuca sativa*, *B. napus*, *T. aestivum*, *B. pekinensis*, *N. benthamian*, and *Lycopersicon esculentum* leaves were tested under ambient environmental conditions. Figure 5 (D) showed that the maximum retention of MT NPs on the surface of plant leaves was higher than that of MYC and TA because of low surface tension. Therefore, MT NPs with excellent surface activity can promote the retention of MYC on the surface of plants without the presence of surfactants.

3.8 Release behavior

Figure 6 shows the release behaviors of MT NPs at different molar ratios of MYC to TA under different pH values. The results showed that the release rate of MYC from MT NPs increased with a decrease in the molar ratio of MYC to TA under the same pH, which might be ascribed to a thicker shell material caused by the lower molar ratio of MYC to TA. The cumulative release of MYC did not increase after 100 h under all conditions, which suggested that there was a balance between assembly and subassembly. The order of release rate of MYC from MT NPs with the same molar ratio of MYC to TA was pH 5, pH 7, and pH 9, indicating that the release rate of MYC under acid conditions was faster than that under neutral and base conditions. The cumulative release data of MYC were fitted to the Ritger–Peppas model (Table 1), and there was a good correlation between the release curve of MYC and the kinetic equation $Mt/Mz = kt^n$ ($r^2 > 0.9$), where n values revealed the mechanism of the release. In the kinetic equation of MT NPs with different molar ratios of MYC to TA and different pH, n values < 0.45 indicated that the release mechanism of MT NPs followed a diffusion-controlled drug release. Therefore, the release of active ingredients from MT NPs could be regulated by changing the molar ratio of MYC to TA and the pH.

3.9 Rainfastness

The rainfastness of MT NPs was evaluated in the laboratory using a simulated rain-washing method (Fig. 7(A)). The retention rates of two formulations on *T. aestivum* leaves after rinsing for 0, 40, 50, and 60 min are shown in Fig. 7(B). The results indicated that

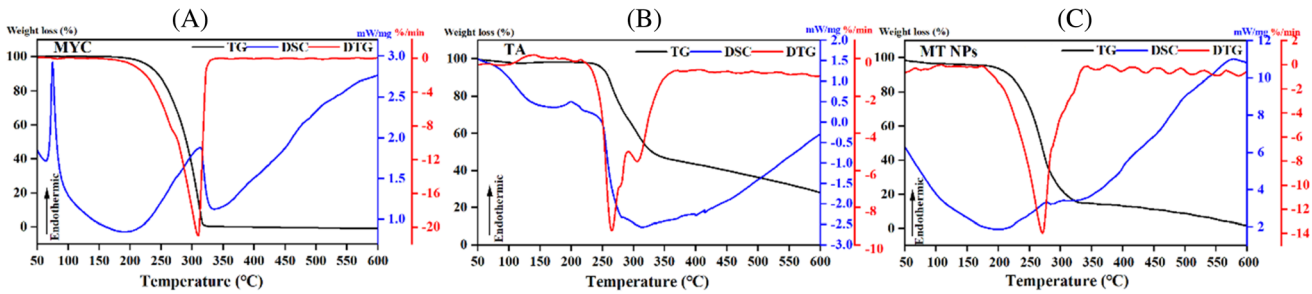

Figure 3. Thermogravimetry (TG), differential thermogravimetric analysis (DTG), and differential scanning calorimetry (DSC) curves of myclobutanil (MYC) (A), tannic acid (TA) (B), and carrier-free co-assembled nanoparticles (MT NPs) (C).

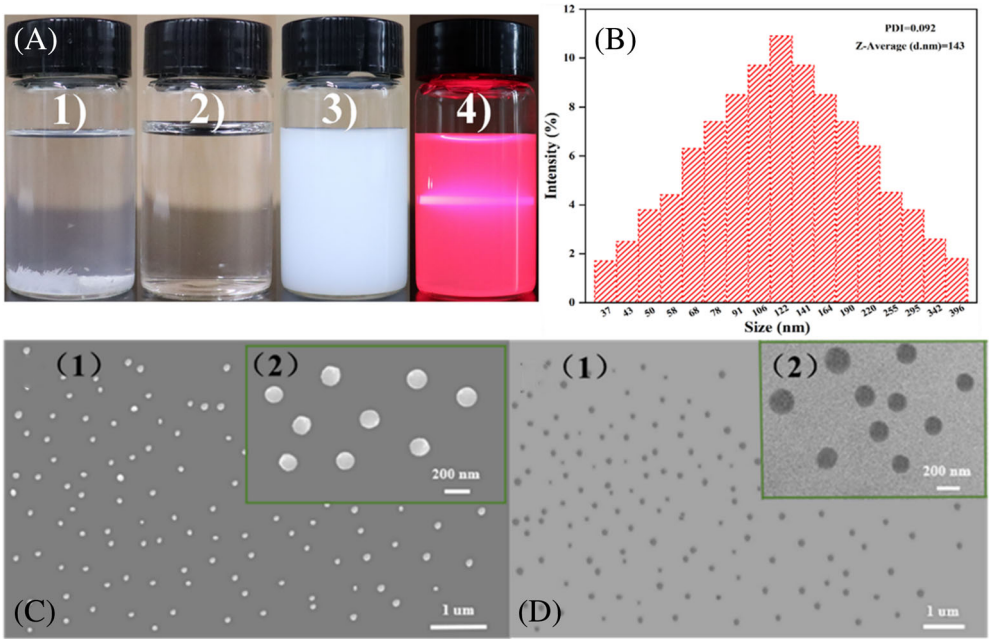

Figure 4. (A) Photographs of aqueous solutions of myclobutanil (MYC) (1), tannic acid (TA) (2), and carrier-free co-assembled nanoparticles (MT NPs) (3) as well as the Tyndall effect of carrier-free co-assembled nanoparticles (MT NPs) in deionized water (4). (B) Particle size distribution of prepared MT NPs measured by laser particle size analyzer. (C) Scanning electron microscopy image of MT NPs (1) and the enlarged image (2). (D) Transmission electron microscopy image of MT NPs (1) and the enlarged image (2).

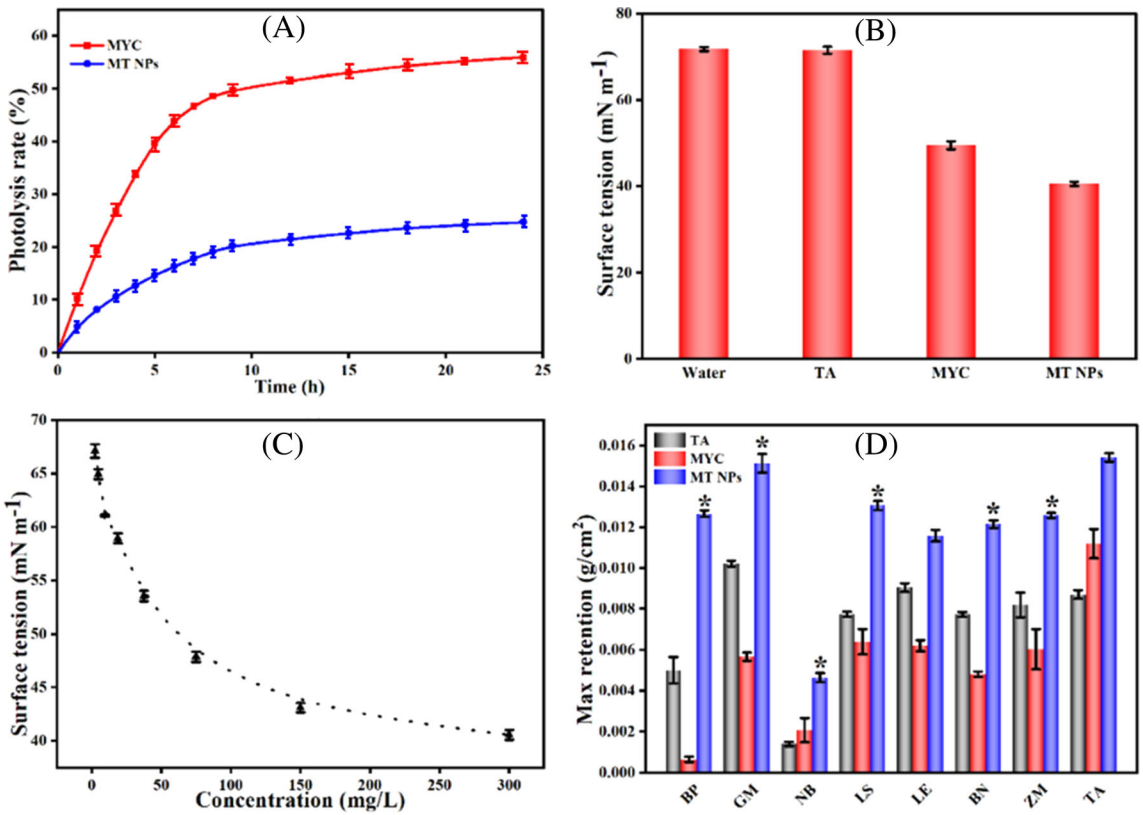

Figure 5. (A) Light stability of myclobutanil (MYC) and carrier-free co-assembled nanoparticles (MT NPs) in water. (B) Surface tensions of aqueous solutions or suspensions of tannic acid (TA), MYC, and MT NPs. (C) Surface tension curve based on concentration of MT NPs. (D) Max retentions of TA, MYC, and MT NPs on different plant leaves. BN, *Brassica napus*; BP, *Brassica pekinensis*; GM, *Glycine max*; LE, *Lycopersicon esculentum*; LS, *Lactuca sativa*; NB, *Nicotiana benthamian*; TA, *Triticum aestivum*; ZM, *Zea mays*.

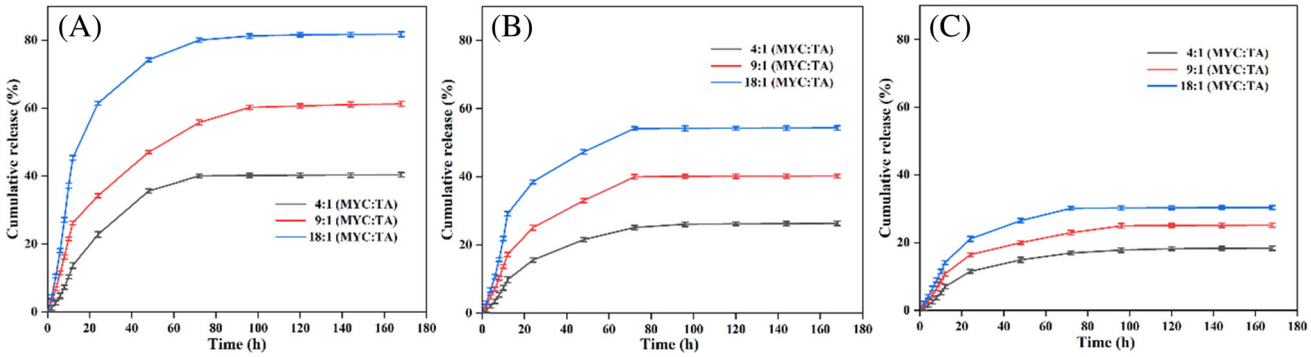

Figure 6. Release behaviors of carrier-free co-assembled nanoparticles (MT NPs) with different molar ratios of myclobutanil (MYC) to tannic acid (TA) at different pH values: pH 5.0 (A), pH 7.0 (B), and pH 9.0 (C).

Table 1. Constants from fitting the generalized model, $M_t/M_z = kt^n$, to the release data of myclobutanil with different molar ratios of myclobutanil to tannic acid at different pH values.

pH	Molar ratio	*n*	*k*	r^2	T_{50} (h)
5	4:1	0.43	4.78	0.9012	214.32
	9:1	0.37	9.91	0.9228	72.28
	18:1	0.38	13.15	0.9176	32.81
7	4:1	9.43	2.82	0.9290	247.20
	9:1	0.44	4.97	0.9476	195.18
	18:1	0.37	8.41	0.9017	118.02
9	4:1	0.35	3.21	0.9098	889.39
	9:1	0.44	2.84	0.9509	475.97
	18:1	0.33	6.35	0.9042	378.48

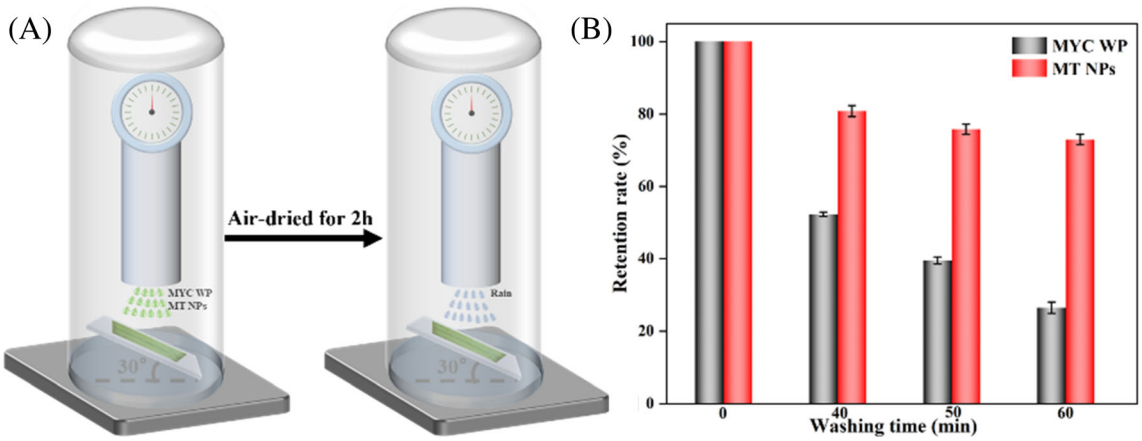

Figure 7. (A) Schematic of measurement of rainfastness by simulated rain-washing method. (B) Retention rates of myclobutanil on *Triticum aestivum* leaf after being washed for 0, 40, 50, and 60 min.

the retention rates of the two formulations were negatively related to rinsing times, and MT NPs had much higher retention rates on *T. aestivum* leaves compared with MYC WP after being washed with water for different times. After being rinsed at 40, 50, and 60 min, the retention rates of MYC WP on *T. aestivum* leaf were 52.3%, 39.5%, and 26.5%, respectively, whereas the retention rates of MT NPs were 80.8%, 75.7%, and 72.9% on *T. aestivum* leaves. Therefore, there were strong interactions between MT NPs and the surface of *T. aestivum* leaf, suggesting excellent rainfastness and highly effective utilization of MT NPs in agricultural production.

3.10 Bioactivity

3.10.1 In vitro *fungicidal activity*

The toxicity regression equations and EC_{50} values of MYC, TA, and MT NPs against *Alternaria alternata* and *F. graminearum* are given in Table 2. For *A. alternata*, the EC_{50} value was highest for TA, followed by MYC, M + T MIX, and MT NPs. For *F. graminearum*, the

Table 2. Antimicrobial activities of tannic acid (TA), myclobutanil (MYC), M + T MIX, and carrier-free co-assembled nanoparticles (MT NPs) against *Alternaria alternata* and *Fusarium graminearum*

	Alternaria alternata				*Fusarium graminearum*			
Drugs	Toxicity equation	r^2	EC_{50} (mg/L)	CTC[a]	Toxicity equation	r^2	EC_{50} (mg/L)	CTC[a]
TA	$y = 0.2784x + 3.4615$	0.9777	251.19	—	$y = 0.491x + 1.9449$	0.9556	503.81	—
MYC	$y = 0.5746x + 3.5985$	0.8762	11.46	—	$y = 0.9177x + 0.5704$	0.9685	124.82	—
M + T MIX	$y = 0.5746x + 3.5985$	0.9162	9.62	194.5	$y = 0.9136x + 0.5104$	0.9937	136.21	179.2
MT NPs	$y = 0.9158x + 3.6713$	0.8411	6.40	313.8	$y = 0.9486x + 0.8785$	0.9873	77.08	240.2

[a] CTC, co-toxicity coefficient; EC_{50}, half-maximal effective concentration.

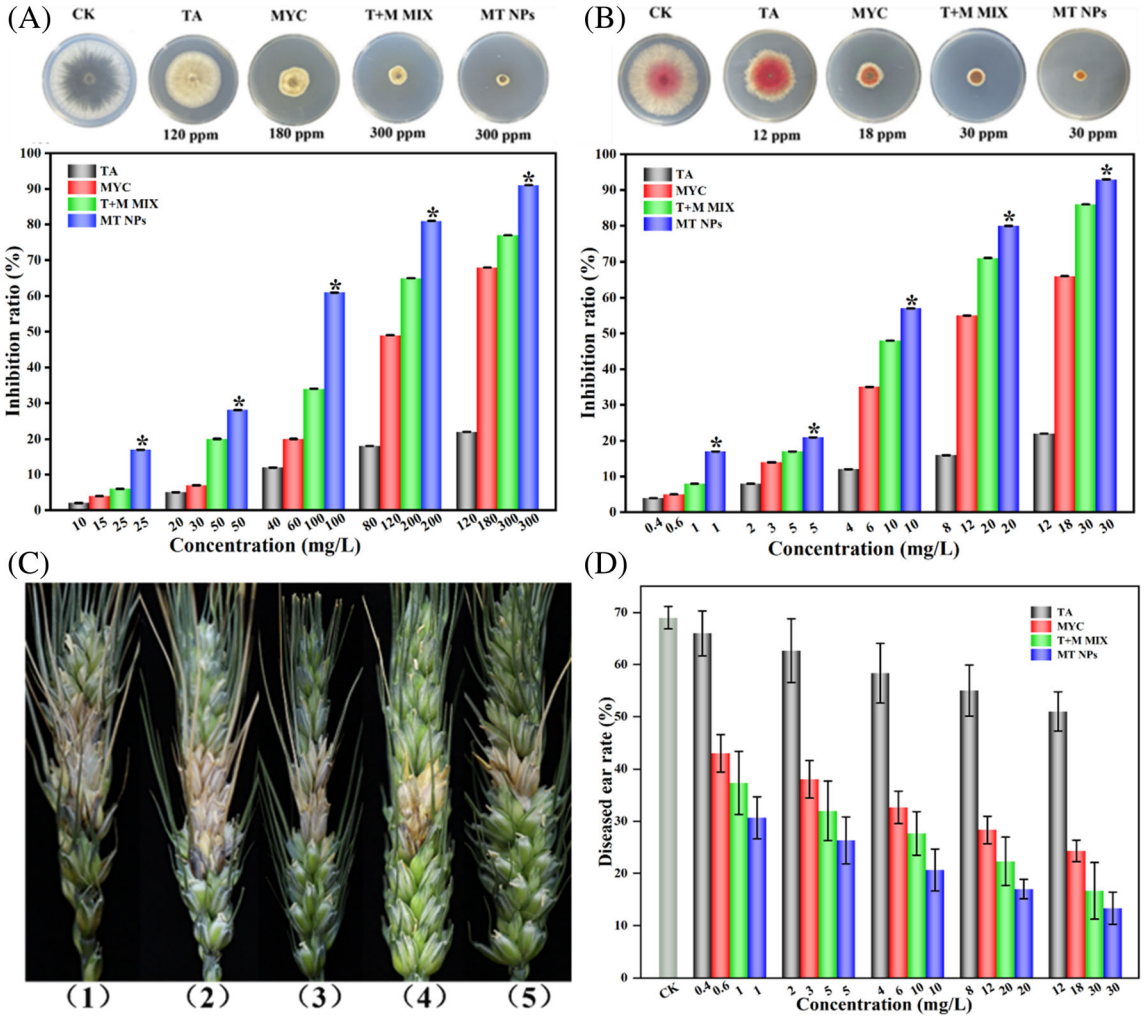

Figure 8. Antimicrobial activities of tannic acid (TA), myclobutanil (MYC), T + M MIX, and carrier-free co-assembled nanoparticles (MT NPs) against *Alternaria alternate* (A) and *Fusarium graminearum* (B). (C) Photographs of diseased wheat ears with different treatments 21 days after being inoculated with *F. graminearum* (1, water; 2, TA at a concentration of 12 mg/L; 3, MYC at a concentration of 18 mg/L; 4, M + T MIX at a concentration of 30 mg/L; MT NPs at a concentration of 30 mg/L). (D) Diseased ear rates on wheat with different treatments at 21 days after being inoculated with *F. graminearum*.

EC_{50} values of TA, MYC, M + T MIX, and MT NPs were 503.81, 124.82, 136.21, and 77.08 mg/L, respectively. The co-toxicity coefficients of MT NPs with a molar ratio of MYC to TA of 9:1 were higher than that of a mixture of MYC and TA at the same molar ratio of MYC to TA, which showed that the fungicidal activity of MT NPs was much better than that of TA, MYC and M + T MIX, the formation of MT NPs containing MYC and TA had a synergistic effect, and the amount of MYC used to control *A. alternata* and *F. graminearum* could be reduced (Fig. 8).

3.10.2 In vivo *control efficacy*

Figure 8(C) shows photographs of diseased wheat ears under different treatments at 21 days after inoculation with *F. graminearum*. The results showed that the order of infection degree in wheat seedling

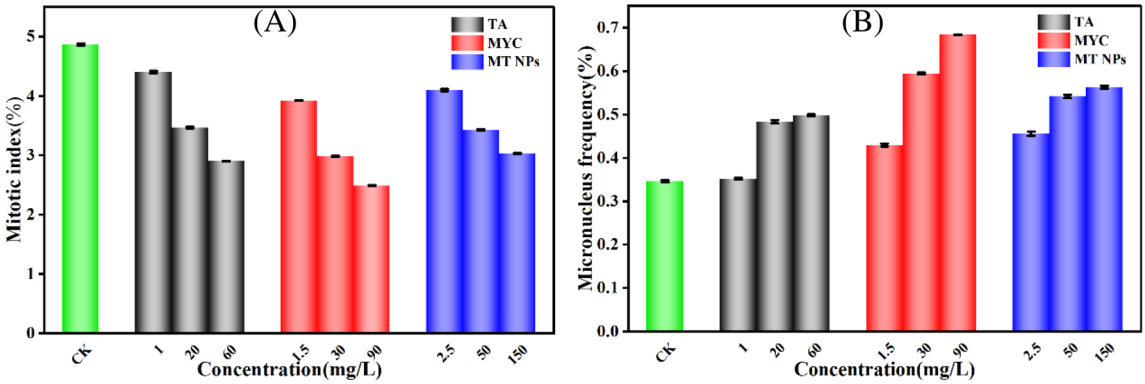

Figure 9. Mitotic index (A) and micronucleus frequency (B) of the root tip cells of *Vicia faba* treated with different concentrations of tannic acid (TA), myclobutanil (MYC), and carrier-free co-assembled nanoparticles (MT NPs).

ears was: water, TA at a concentration of 12 mg/L, MYC at a concentration of 18 mg/L, M + T MIX at a concentration of 30 mg/L, and MT NPs at a concentration of 30 mg/L. Figure 8(D) gives the diseased seedling ear rates for TA, MYC, M + T MIX, and MT NPs at different concentrations against *F. graminearum*. The diseased seedling ear rates of TA, MYC, M + T MIX, and MT NPs at concentrations of 12, 18, 30, and 30 mg/L were 51.0%, 24.33%, 16.67%, and 13.33% respectively, suggesting that the combination of MYC and TA by the co-assembly method had a synergistic effect on the antifungal activity against *F. graminearum*. Therefore, MT NPs co-assembled by MYC and TA with improved fungicidal activity are an alternative for the management of disease in wheat seedlings.

3.11 Genotoxicity

The biosafety of MT NPs was demonstrated by the mitotic index (proportion of dividing cells) and micronucleus frequency of *V. faba* root tip cells. The mitotic index and micronucleus frequency of *V. faba* root tip cells treated with MYC, TA, and MT NPs at various concentrations are shown in Fig. 9. The mitotic index of *V. faba* root tip cells was higher with MT NPs treatment than with the TA and MYC treatments, showing that the MT NPs had less effect on chromosome division in *V. faba* root tip cells at experimental concentrations. Figure 9(B) gives the micronucleus frequencies of *V. faba* root tip cells treated with different concentrations of MYC, TA, and MT NPs. The micronucleus rates of *V. faba* root tip cells treated with MYC at concentrations of 30 and 90 mg/L were higher than with MT NPs at concentrations of 50 and 150 mg/L. In general, the higher the micronucleus frequency, the greater the genotoxicity caused by the samples. Therefore, co-assembly could reduce the genotoxicity of MYC to *V. faba* and MT NPs posed a low risk to *V. faba* cells.

4 CONCLUSIONS

In summary, carrier-free co-assembled MT NPs based on MYC and the natural fungicide TA were prepared using a green preparation process. Laser particle-size analyzer, SEM, TEM, HPLC, UV-visible absorbance spectra, FTIR spectra, ^{1}H NMR spectra, TG analysis, and surface tension measurements were used to characterize the obtained MT NPs. The results indicated that the optimal molar ratio of MYC to TA was 9:1 in aqueous solution at pH 5 and 25 °C, and the salt concentration had no obvious effect on the co-assembly. The obtained MT NPs had good physical and chemical properties, uniform morphology (143 nm), a low PDI (0.092), and remarkable stability. The release of active ingredients from MT NPs could be regulated by changing the molar ratios of MYC to TA and the pH. The results showed that MT NPs had much better antifungal activity than free MYC, TA, and MYC + TA MIX, and showed a synergistic antifungal activity with MYC and TA incorporated in nanoparticles. A genotoxicity evaluation indicated that co-assembled MT NPs could reduce the genotoxicity of MYC to plant cells. Therefore, carrier-free co-assembled MT NPs with synergistic antifungal activity developed using an environmentally friendly preparation process have excellent potential for the sustainable management of plant diseases.

ACKNOWLEDGEMENTS

The authors acknowledge financial support of this work by Beijing Agriculture Innovation Consortium (BAIC02-2022) and Sanya Yazhou Bay Science and Technology City (grant numbers SYND-2022-05).

CONFLICT OF INTEREST

The authors declare no competing financial interest.

DATA AVAILABILITY STATEMENT

The data that support the findings of this study are available from the corresponding author upon reasonable request.

REFERENCES

1 Chen L, Lin YX, Zhou HJ, Hao L, Chen HY and Zhou XH, A stable polyamine-modified zein-based nanoformulation with high foliar affinity and lowered toxicity for sustained avermectin release. *Pest Manag Sci* **77**:3300–3312 (2021).
2 Yan WY, Fu X, Gao Y, Shi LY, Liu Q, Yang WC *et al.*, Synthesis, antibacterial evaluation, and safety assessment of CuS NPs against Pectobacterium carotovorum subsp. carotovorum. *Pest Manag Sci* **78**:733–742 (2022).
3 Liu Y, Sun Y, He S, Zhu YC, Ao MM, Li JQ *et al.*, Synthesis and characterization of gibberellin-chitosan conjugate for controlled-release applications. *Int J Biol Macromol* **57**:213–217 (2013).
4 Zhang WB, Shi TY, Ding GL, Punyapitak D, Zhu JL, Guo D *et al.*, Nanosilica schiff-base copper (II) complexes with sustainable antimicrobial activity against bacteria and reduced risk of harm to plant and environment. *ACS Sustainable Chem Eng* **5**:502–509 (2017).
5 Fan C, Guo MC, Liang Y, Dong HQ, Ding GL, Zhang WB *et al.*, Pectin-conjugated silica microcapsules as dual-responsive carriers for increasing the stability and antimicrobial efficacy of kasugamycin. *Carbohydr Polym* **172**:322–331 (2017).

6 Liang Y, Guo MC, Fan C, Dong HQ, Ding GL, Zhang WB *et al*., Development of novel urease-responsive pendimethalin microcapsules using silica-IPTS-PEI as controlled release carrier materials. *ACS Sustain Chem Eng* **5**:4802–4810 (2017).
7 He S, Zhang WB, Li DG, Li PL, Zhu YC and Ao MM, Li JQ amd Cao YS, preparation and characterization of double-shelled avermectin microcapsules based on copolymer matrix of silica–glutaraldehyde–chitosan. *J Mat Chem B* **1**:1270–1278 (2013).
8 Liu Y, Sun Y, Ding GL, Geng QQ, Zhu JL, Guo MC *et al*., Synthesis, characterization, and application of microbe-triggered controlled-release kasugamycin pectin conjugate. *J Agric Food Chem* **63**:4263–4268 (2015).
9 Liang Y, Song JH, Dong HQ, Huo ZY, Gao YH, Zhou ZY *et al*., Fabrication of pH-responsive nanoparticles for high efficiency pyraclostrobin delivery and reducing environmental impact. *Sci Total Environ* **787**: 147422 (2021).
10 Zhang WB, He S, Liu Y, Geng QQ, Ding GL, Guo MC *et al*., Preparation and characterization of novel functionalized prochloraz microcapsules using silica–alginate–elements as controlled release carrier materials. *ACS Appl Mater Interfaces* **6**:11783–11790 (2014).
11 Guo MC, Zhang WB, Ding GL, Guo D, Zhu JL, Wang BT *et al*., Preparation and characterization of enzyme-responsive emamectin benzoate microcapsules based on a copolymer matrix of silica–epichlorohydrin–carboxymethylcellulose. *RSC Adv* **5**:93170–93179 (2015).
12 Liang Y, Fan C, Dong HQ, Zhang WB, Tang G, Yang JL *et al*., Preparation of MSNs-chitosan@ Prochloraz nanoparticles for reducing toxicity and improving release properties of prochloraz. *ACS Sustain Chem Eng* **6**:10211–10220 (2018).
13 Tang JY, Ding GL, Niu JF, Zhang WB, Tang G, Liang Y *et al*., Preparation and characterization of tebuconazole metal-organic framework-based microcapsules with dual-microbicidal activity. *Chem Eng J* **359**:225–232 (2019).
14 Tang JY, Tang G, Niu JF, Yang JL, Zhou ZY, Gao YH *et al*., Preparation of a porphyrin metal–organic framework with desirable photodynamic antimicrobial activity for sustainable plant disease management. *J Agric Food Chem* **69**:2382–2391 (2021).
15 Niu JF, Tang G, Tang JY, Yang JL, Zhou ZY, Gao YH *et al*., Functionalized silver nanocapsules with improved antibacterial activity using silica shells modified with quaternary ammonium polyethyleneimine as a bacterial cell-targeting agent. *J Agric Food Chem* **69**:6485–6494 (2021).
16 Zhao M, Zhou HJ, Hao L, Chen H and Zhou XH, A high-efficient nano pesticide-fertilizer combination fabricated by amino acid-modified cellulose based carriers. *Pest Manag Sci* **78**:506–520 (2022).
17 Datta S, Misra SK, Saha ML, Lahiri N, Louie J, Pan D *et al*., Orthogonal self-assembly of an organoplatinum (II) metallacycle and cucurbit [8] uril that delivers curcumin to cancer cells. *Proc Natl Acad Sci U S A* **115**:8087–8092 (2018).
18 Quiñones JP, Peniche H and Peniche C, Chitosan based self-assembled nanoparticles in drug delivery. Chitosan based self-assembled nanoparticles in drug delivery. *Polymers* **10**:235 (2018).
19 Castelletto V, Edwards-Gayle CJ, Greco F, Hamley IW, Seitsonen J and Ruokolainen J, Self-assembly, tunable hydrogel properties, and selective anti-cancer activity of a carnosine-derived lipidated peptide. *ACS Appl Mater Interfaces* **11**:33573–33580 (2019).
20 Delfi M, Sartorius R, Ashrafizadeh M, Sharifi E, Zhang YP, De Berardinis P *et al*., Self-assembled peptide and protein nanostructures for anti-cancer therapy: targeted delivery, stimuli-responsive devices and immunotherapy. *Nano Today* **38**:101119 (2021).
21 Sabra S, Abdelmoneem M, Abdelwakil M, Mabrouk MT, Anwar D, Mohamed R *et al*., Self-assembled nanocarriers based on amphiphilic natural polymers for anti-cancer drug delivery applications. *Curr Pharm Design* **23**:5213–5229 (2017).
22 Narayan T, Kumar S, Kumar S, Augustine S, Yadav BK and Malhotra BD, Protein functionalised self assembled monolayer based biosensor for colon cancer detection. *Talanta* **201**:465–473 (2019).
23 Tang G, Tian Y, Gao YH, Zhou ZY, Chen X, Li Y *et al*., Supramolecular self-assembly of herbicides with reduced risks to the environment. *ACS Nano* **16**:4892–4904 (2022).
24 Tang G, Tian YY, Niu JF, Tang JY, Yang JY, Gao YH *et al*., Development of carrier-free self-assembled nanoparticles based on fenhexamid and polyhexamethylene biguanide for sustainable plant disease management. *Green Chem* **23**:2531–2540 (2021).
25 Tian YY, Tang G, Li Y, Zhou ZY, Chen X, Gao YH *et al*., A simple preparation process for an efficient nano-formulation: small molecule self-assembly based on spinosad and sulfamic acid. *Green Chem* **23**: 4882–4891 (2021).
26 Tian YY, Tang G, Gao YH, Chen X, Zhou ZY, Li Y *et al*., Carrier-free small molecular self-assembly based on Berberine and curcumin incorporated in submicron particles for improving antimicrobial activity. *ACS Appl Mater Interfaces* **14**:10055–10067 (2022).
27 Tian YY, Zhang XH, Huang YQ, Tang G, Gao YH, Chen X *et al*., Amphiphilic prodrug nano-micelles of fipronil coupled with natural carboxylic acids for improving physicochemical properties and reducing the toxicities to aquatic organisms. *Chem Eng J* **439**:135717 (2022).
28 Tian YY, Huang YQ, Zhang XH, Tang G, Gao YH, Zhou ZY *et al*., Self-assembled nanoparticles of prodrug conjugate based on pyrimethanil for efficient plant disease management. *J Agric Food Chem* **70**: 11901–11910 (2022).
29 Bonde MR, Peterson GL, Rizvi SA and Smilanick JL, Myclobutanil as a curative agent for chrysanthemum white rust. *Plant Dis* **79**:500505 (1995).
30 European Food Safety Authority, Conclusion on the peer review of the pesticide risk assessment of the active substance myclobutanil. *EFSA J* **8**:1682 (2010).
31 Pandiselvam R, Kaavya R, Jayanath Y, Veenuttranon K, Lueprasitsakul P, Divya V *et al*., Ozone as a novel emerging technology for the dissipation of pesticide residues in foods–a review. *Trends Food Sci Technol* **97**:38–54 (2020).
32 Garcia-Muñoz P, Dachtler W, Altmayer B, Schulz R, Robert D, Seitz F *et al*., Reaction pathways, kinetics and toxicity assessment during the photocatalytic degradation of glyphosate and myclobutanil pesticides: influence of the aqueous matrix. *Chem Eng J* **384**:123315 (2020).
33 Kaczmarek B, Tannic acid with antiviral and antibacterial activity as a promising component of biomaterials—a minireview. *Materials* **13**: 3224 (2020).
34 Yeo J, Lee J, Yoon S and Kim WJ, Tannic acid-based nanogel as an efficient anti-inflammatory agent. *Biomater Sci* **8**:1148–1159 (2020).
35 Yang G, Fang DF, Yang LM, Wei ZM, Tu YY, Shao PH *et al*., Tailored construction of β-cyclodextrin covalently-supported tannic acid polymer nanosponge towards highly selective lead recovery. *J Clean Prod* **330**:129882 (2022).
36 Shin M, Park E and Lee H, Plant-inspired pyrogallol-containing functional materials. Plant-inspired pyrogallol-containing functional materials. *Adv Funct Mater* **29**:1903022 (2019).
37 Gao XJ, Dai QY, Yao LT, Dong H, Li QT and Cao XD, A medical adhesive used in a wet environment by blending tannic acid and silk fibroin. *Biomater Sci* **8**:2694–2701 (2020).
38 Brzeziński M, Socka M, Makowski T, Kost B, Cieślak M and Królewska-Golińska K, Microfluidic-assisted nanoprecipitation of biodegradable nanoparticles composed of PTMC/PCL (co) polymers, tannic acid and doxorubicin for cancer treatment. *Colloid Surf B-Biointerfaces* **201**:111598 (2021).
39 Ejima H, Richardson JJ and Caruso F, Metal-phenolic networks as a versatile platform to engineer nanomaterials and biointerfaces. *Nano Today* **12**:136–148 (2017).
40 Yan WT, Shi MQ, Dong CX, Liu LF and Gao CJ, Applications of tannic acid in membrane technologies: a review. *Adv Colloid Interface Sci* **284**:102267 (2020).
41 Ren JL, Kong RX, Gao YJ, Zhang LB and Zhu JT, Bioinspired adhesive coatings from polyethylenimine and tannic acid complexes exhibiting antifogging, self-cleaning, and antibacterial capabilities. *J Colloid Interface Sci* **602**:406–414 (2021).
42 Wang M, Sun X, Zhong NQ, Cai DQ and Wu ZY, Promising approach for improving adhesion capacity of foliar nitrogen fertilizer. *ACS Sustain Chem Eng* **3**:499–506 (2015).
43 Niu JF, Tang JY, Tang G, Zhou ZY, Tang R, Yang JL *et al*., Enhanced phototherapy activity by employing a Nanosilica-Coumarin–Acifluorfen conjugate as the supplementary light source generator. *ACS Sustain Chem Eng* **7**:17706–17713 (2019).

